Title

Behavior of soda-lime silicate glass under laser-driven shock compression up to 315 GPa

Authors

Madhavi, Meera
Jangid, Rahul
Christiansen-Salameh, Joyce
et al.

Behavior of soda-lime silicate glass under laser-driven shock compression up to 315 GPa

Meera Madhavi; Rahul Jangid; Joyce Christiansen-Salameh; ... et. al

Check for updates

CrossMark

View Online   Export Citation

Articles You May Be Interested In

Behavior of soda-lime silicate glass under laser-driven shock compression up to 315 GPa

Meera Madhavi,[1] Rahul Jangid,[1] Joyce Christiansen-Salameh,[1] Yu-Hsing Cheng,[1] Pooja Rao,[1] Jianheng Li,[1] Surya Teja Botu,[1] Spencer Jeppson,[1] Jugal Mehta,[1] Scott Smith,[1] Jared T. Isobe,[2] Sovanndara Hok,[3] Rahul Saha,[4] Eric Cunningham,[5] Philip Heimann,[5] Dimitri Khaghani,[5] Hae Ja Lee,[5] D. K. Spaulding,[6] Danae N. Polsin,[7] Arianna E. Gleason,[5] and Roopali Kukreja[1,a]

AFFILIATIONS

[1]Department of Materials Science and Engineering, University of California Davis, Davis, California 95616, USA
[2]Department of Geophysics, Stanford University, 397 Panama Mall, Stanford, California 94305, USA
[3]Department of Geological Sciences, Stanford University, 450 Jane Stanford Way, Bldg. 320 Rm. 118, Stanford, California 94305, USA
[4]Department of Physics and Astronomy, University of Rochester, 206 Bausch and Lomb Hall, Rochester, New York 14627-0171, USA
[5]SLAC National Accelerator Laboratory, 2575 Sand Hill Road, Menlo Park, California 94025, USA
[6]Department of Earth and Planetary Sciences, University of California, Davis, California 95616, USA
[7]Laboratory for Laser Energetics, 250 E. River Rd., Rochester, New York 14623, USA

[a]**Author to whom correspondence should be addressed:** rkukreja@ucdavis.edu

ABSTRACT

Shock experiments give a unique insight into the behavior of matter subjected to extremely high pressures and temperatures. Understanding the behavior of materials under such extreme conditions is key to modeling material failure and deformation dynamics under impact. While studies on pure silica are extensive, the shock behavior of other commercial silicates that contain additional oxides has not been systematically investigated. To better understand the role of composition in the dynamic behavior of silicates, we performed laser-driven dynamic compression experiments on soda-lime glass (SLG) up to 315 GPa. Using the accurate pulse shaping offered by the long pulse laser system at the Matter in Extreme Conditions end-station at the Linac Coherent Light Source, SLG was shock compressed along the Hugoniot to multiple pressure-temperature points. Velocity Interferometer System for Any Reflector was used to measure the velocity and determine the pressure inside the SLG. The U_s–u_P relationship obtained agrees well with the previous parallel plate impact studies. Within the error bars, no transformation to the crystalline phase was observed up to 70 GPa, which is in contrast to the behavior of pure silica under shock compression. Our studies show that the glass composition strongly influences the shock compression behavior of the silicate glasses.

Published under an exclusive license by AIP Publishing. https://doi.org/10.1063/5.0132114

I. INTRODUCTION

Silicate glasses are an integral part of the modern society with applications in electronics, housing, communication technologies, and terrestrial and space vehicles. They are of particular importance in military and space applications, where shuttle or aircraft windows can undergo high-energy ballistic impacts and encounter high-speed debris from micro-meteorites or broken satellite fragments or as the space shuttle reenters the Earth's atmosphere.[1] These high-energy impacts are characterized by high pressures, temperatures, and strain rates. Silicate glasses are also used in high-power lasers as optical elements, in optical fibers, and as screens where they are often under thermal or mechanical stress. Under such dynamic loading conditions, pressure or strain-driven shock waves in solid materials can result in damage and deformation.[2,3] In order to assess and reduce the risk of damage that can cause structural failure, the behavior of glass under high pressure or strain rate conditions must be accurately studied using experimental and theoretical techniques. Understanding the behavior of various silicate glasses under dynamic compression would allow us to not only predict their behavior under high-energy impacts but will also allow us to establish a composition and network structure that can best sustain impacts without significant loss in transparency and

strength.[2,3] Furthermore, silicate glasses at high pressures are used as model systems for understanding melts and liquids in planetary interiors.

Silicate glasses contain silica (SiO_2) as the main component with varied amounts of additional oxides. The structure of a typical silicate glass can be explained using the random network model where Si-oxygen polyhedra are connected through corner-sharing oxygen atoms to form a 3D network.[3,4] The oxygen polyhedra are usually trigonal planar or tetrahedral around the network forming cation. The network structure and, therefore, the behavior of the silicate glasses can be modified by changing the composition. The additional cations in the silicate glass can either act as a network former (B, Al, etc.) or a network modifier (Na, Ca, etc.). A network modifier breaks the network connectivity, creating a more open structure while a network former replaces Si and maintains the network connectivity to an extent. Understanding how the composition and network structure influences the dynamic response of silicate glasses is critical for tailoring and developing specific compositions based on required applications. Fused silica (FS), the simplest silicate glass consisting of only SiO_2, is typically used in space shuttles as it has a high thermal resistance and can withstand the extreme conditions during shuttle reentry. However, high purity fused silica is very expensive. Recent studies on fused silica observed the formation of crystalline stishovite upon shock compression.[1,5] While the dynamic response of fused silica has been studied extensively, the dynamic response of other silicate glasses, such as soda-lime glass (SLG), or borosilicate glass has not yet been systematically explored.

In this study, we report the dynamic behavior of SLG under laser-driven shock compression up to 315 GPa. The additional Na^+ and Ca^{2+} cations in the SLG break the Si–O–Si network connectivity leading to a more open structure with more non-bridging oxygen ions. Hugoniot measurements were performed using the long pulse optical laser at the Matter in Extreme Conditions (MEC) hutch at the Linac Coherent Light Source (LCLS). MgO and Lithium Fluoride (LiF) were used as the window material and as the standard for impedance matching. The velocity interferometer system for any reflector (VISAR) was used to measure the particle velocity at the Kapton (ablator)/SLG interface and the SLG/MgO (or LiF) window interface.[6–8] A U_s–u_p relationship was obtained for the laser-driven shock studies and was compared to those from parallel plate impact studies. Comparison with previous studies on fused silica (FS) showed that in contrast with transformation to stishovite for pure FS, no amorphous to crystalline transformation is observed for SLG within the error bars up to 70 GPa.

II. EXPERIMENTAL METHODS

$2 \times 2\,mm^2$ double-side parallel-polished SLG of thickness $50\,\mu m$ and density $2.53\,g/cm^3$ was obtained from Asphera Inc. The composition of SLG was measured using an Electron Probe Micro Analyzer (EPMA) to be 72.7% SiO_2, 12.9% Na_2O, 10.2% CaO, 2.9% of MgO. The refractive index was measured to be 1.521 by observing the Becke line under an optical microscope with the sample immersed in oils of known refractive index. Two experimental target stacks were used for the measurement. For stack 1, as shown in Fig. 1(a), the SLG samples were glued to a $25\,\mu m$ thick

Kapton B polyimide ablator using Hardman double bubble fast set epoxy glue. A 200 nm Al layer was deposited on the ablator, facing the laser drive, to prevent pre-shock from the tails of the laser pulse. A 100 nm Au layer was deposited in the Kapton/SLG interface on the SLG side as a reflecting surface for VISAR laser to measure the interface particle velocity following the shock wave entry. The glass samples were then glued to a LiF window of thickness $100–150\,\mu m$, which was used as the standard with a known equation of state (EOS). A 100 nm Al layer was deposited at the SLG/LiF interface on one-half of LiF window, which also acted as a reflecting surface for the VISAR. The thickness of each SLG sample and LiF window was measured prior to the build. The thickness of the stack was measured after each gluing stage. A total glue thickness of $0–5\,\mu m$ was measured with the individual glue thickness at the Kapton/SLG side varying from 0 to $2\,\mu m$ and the glue thickness on the SLG/LiF varying from 0 to $3\,\mu m$. This was measured for each stack and was included in the U_s-u_p calculations. The error in thickness measurement was $0.5\,\mu m$.

Figure 1(b) also shows a VISAR image captured during shock compression of SLG in the stack 1 geometry. The VISAR images for all the stack 1 data are shown in Sec. S1 in the supplementary material. The shock breakout into the interfaces is characterized by the motion in the VISAR fringes. There are two breakouts corresponding to the two reflecting surfaces. The first breakout (yellow dashed line) corresponds to the shock front entering the SLG through the Kapton/SLG interface and the second breakout (white dashed line) corresponds to the shock front exiting the SLG into the LiF window through the SLG/LiF interface. The difference between the breakout times can be used to estimate the transit time through the glass.

Stack 2, shown in Fig. 1(c), consists of SLG samples glued with the epoxy to a $25\,\mu m$ thick Kapton B polyimide ablator with a 200 nm Al layer facing the drive laser. The glass samples were then glued to an MgO window of thickness $500\,\mu m$, which was used as the standard with a known EOS. A 100 nm Al layer was deposited at the SLG/MgO interface on the MgO window side, which acted as a reflecting surface for the VISAR laser to measure the interface particle velocity following the shock wave entry. The MgO window EOS was used to calculate the pressure inside the SLG sample through impedance matching. The total glue layer thickness for the stack 2 geometry was found to vary between 0 and $10\,\mu m$. Figure 1(d) shows the interference image obtained from the 532 nm VISAR beam obtained upon laser-driven shock compression of SLG in target stack 2 geometry. A breakout, characterized by the motion in the VISAR interference fringes, is observed as the shock enters the MgO window from the SLG sample through the SLG/Al/MgO interface. The VISAR images for all the stack 2 data are shown in Sec. S2 in the supplementary material.

The 527 nm Nd:glass long pulse optical laser at the MEC end-station at LCLS was focused to a $300\,\mu m$ (stack 1) and $250\,\mu m$ (stack 2) spot size to drive the shock through the sample. Upon laser irradiation, the ablator produces a self-sustaining plasma that extends outward while simultaneously causing a compression wave to travel through the sample. In this study, we employed a 10 ns flat top pulse (FT 10 ns) for the drive laser. The samples were compressed to multiple pressure-temperature points in the Hugoniot
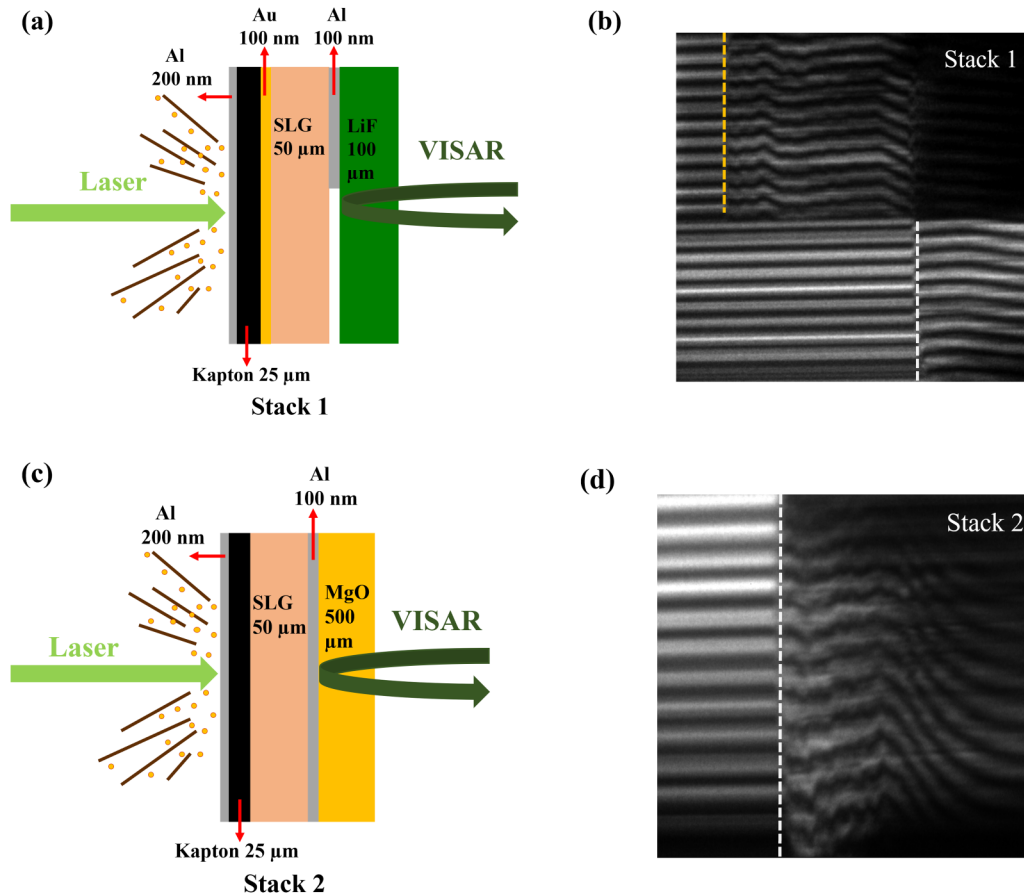
FIG. 1. (a) Experimental target stack 1 geometry for laser-driven shock compression studies performed at MEC end-station at LCLS. The geometry has two reflecting surfaces for VISAR. (b) Representative VISAR image captured during shock compression driven by a flat top 10 ns laser pulse of energy of 27.16 J resulting in a peak stress of 57.13 GPa for stack 1. The yellow dashed line represents the shock breakout into the Kapton/Au/SLG interface as the shock enters the SLG and the white dashed line represents the shock breakout into the SLG/Al/LiF interface as the shock exits the SLG. (c) Experimental target stack 2 geometry. (d) Representative VISAR image captured during shock compression driven by 33.13 J flat top 10 ns laser pulse resulting in a peak stress of 117 GPa for stack 2.

space by changing the drive laser energy. The maximum drive laser energy employed was 60 J leading to a maximum intensity of 1.21×10^{13} W/cm^2 allowing the glass sample to reach pressures up to 315 GPa.

III. EXPERIMENTAL RESULTS AND ANALYSIS

Figure 2 shows the apparent interface particle velocity evolution over time for different pressures inside the SLG sample. The peak particle velocity measured increases as a function of the drive laser energy for stack 1 and stack 2. The shock breakout into the SLG through the Kapton/Au/SLG interface in stack 1 is characterized by a sharp increase in the interface velocity measured from the VISAR. A steady shock is assumed for both stacks. The uncertainties in the particle velocity are obtained from the difference in the interface velocities immediately after the breakout in VISAR1 and VISAR2. The structure of the interface velocity curve could be potentially due to

the structure of the flat top pulse or due to the arrival of edge release waves. For stack 2, the shock was seen to persist for about 5 ns in the samples. This was followed by release resulting in the observed decrease in the interface particle velocity.

The interface velocities were obtained from the magnitude of the fringe shift in the VISAR image using the Igor Pro 8 software and using LLNL's AnalyzeVISAR code.[6–8] The peak interface particle velocity measured immediately after the shock breaks out, which corresponds to the peak position right after the sudden increase in the velocities in Fig. 2, was used in the analysis. This corresponds to interface velocity measured 300 ps after laser shock and includes detector response time, shock laser, and VISAR laser jitter.

For stack 1 geometry, the measured apparent interface particle velocity was corrected for the refractive index using the correction factor[2] to obtain the SLG particle velocity (u_p). To calculate the shock transit time through the SLG, the two breakout times
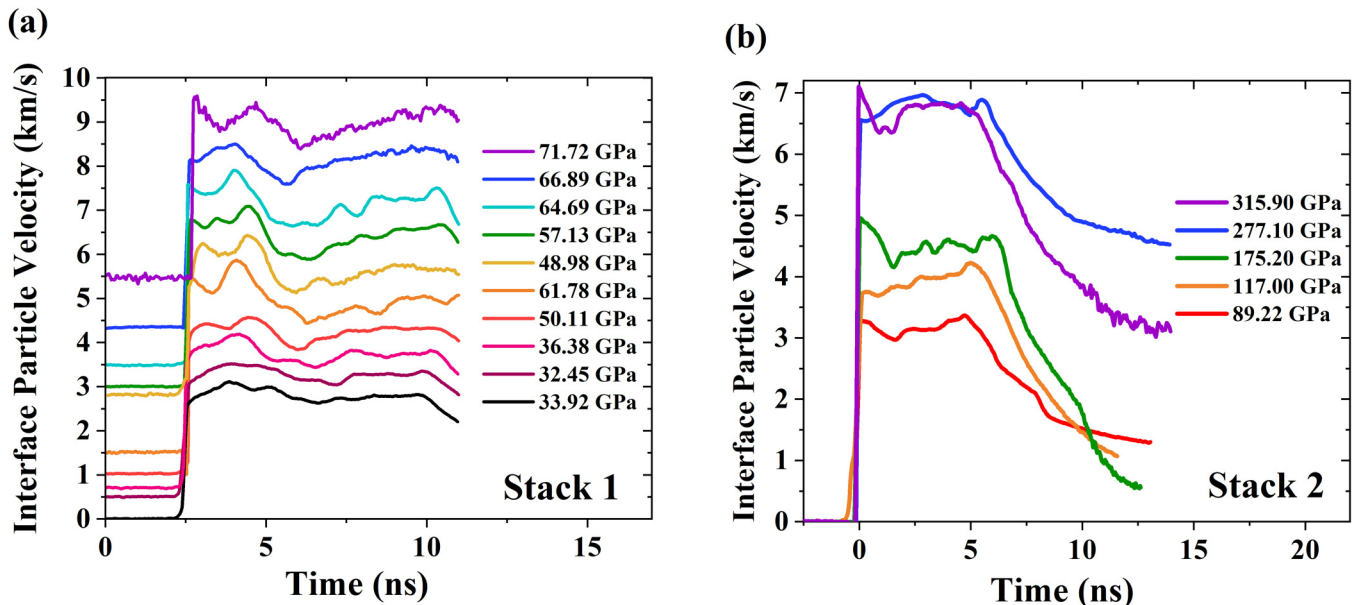
FIG. 2. (a) Time evolution of the apparent Kapton/Au/SLG interface particle velocity for sample stack 1 from shock driven by FT 10 ns pulse with spot size 300 μm. (b) Time evolution of the SLG/Al/MgO interface particle velocity for sample stack 2 from shock driven by FT 10 ns drive laser with spot size 250 μm.

corresponding to when the shock enters the Kapton/Au/SLG interface [dashed yellow line in Fig. 1(b)] and subsequently when shock enters the SLG/Al/LiF interface [dashed white line in Fig. 1(b)] were used. The shock velocity (SLG U_s) was then calculated from
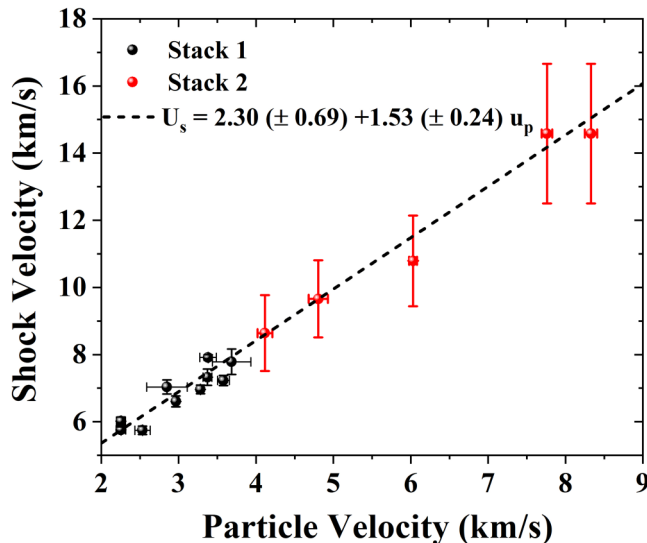
the transit time using the thickness of each SLG sample, which was carefully cataloged before the experiment.

Figure 3 shows the U_s–u_p relationship obtained from our measurements of stack 1 (black points). The fit obtained was

$$U_s = 2.30\,(\pm 0.69) + 1.53\,(\pm 0.24)\,u_p. \qquad (1)$$

The two VISAR setups (i.e., VISAR1 and VISAR2) were seen to have a slight difference in the breakout times and, therefore, the difference in the transit time measured between VISAR1 and VISAR2 was incorporated in the shock velocity error bars. The pressure and the density inside the SLG in stack 1 geometry was obtained using the Rankine Hugoniot equations,[9]

$$P = \rho_o U_s u_p, \qquad (2)$$

$$\rho = \frac{\rho_o U_s}{U_s - u_p}, \qquad (3)$$

where P is the pressure, U_s is the shock velocity, u_p is the particle velocity, ρ_o and ρ are the ambient density and the density of the shocked sample respectively. The volume compression (VC) is given by the equation,

$$VC = \frac{\rho_o}{\rho}, \qquad (4)$$

FIG. 3. Measured shock velocity (U_s) vs particle velocity (u_p) for the SLG. The black points were measured for the sample stack 1 and the red points for the sample stack 2.

The summary of all the shots including the drive laser average intensity, drive laser energy, U_s, u_p, and pressure (P) of samples in stack 1 geometry shock compressed by a 300 μm spot size FT 10 ns pulse is presented in Table I.

TABLE I. Summary of the drive laser energy, average intensity, u_p, U_s, pressure, density, and volume compression results obtained for SLG sample stack 1 compressed by FT 10 ns pulse with a 300 μm spot size.

	Experimental quantities				Calculated in-material quantities		
Energy (J)	Intensity (TW/cm^2)	Apparent interface u_p (Kapton/Au/SLG) (km/s)	SLG u_p (km/s)	SLG U_s (km/s)	SLG pressure (GPa)	Density (g/cm^3)	Volume compression
17.69	2.50	2.62 (0.06)	2.25 (0.06)	6.02 (0.13)	33.92 (1.13)	3.99 (0.10)	0.63 (0.02)
17.86	2.53	2.62 (0.06)	2.25 (0.06)	5.76 (0.09)	32.45 (1.03)	4.11 (0.14)	0.61 (0.02)
20.97	2.97	2.95 (0.11)	2.53 (0.10)	5.75 (0.12)	36.38 (1.62)	4.47 (0.24)	0.56 (0.03)
25.02	3.54	3.31 (0.30)	2.85 (0.26)	7.04 (0.21)	50.11 (4.84)	4.20 (0.36)	0.59 (0.05)
25.42	3.60	3.92 (0.06)	3.37 (0.06)	7.33 (0.24)	61.78 (2.31)	4.64 (0.33)	0.54 (0.04)
26.17	3.70	3.45 (0.01)	2.96 (0.03)	6.61 (0.16)	48.98 (1.29)	4.53 (0.23)	0.55 (0.03)
27.16	3.84	3.82 (0.02)	3.28 (0.04)	6.96 (0.13)	57.13 (1.27)	4.73 (0.19)	0.53 (0.02)
30.89	4.37	4.16 (0.08)	3.58 (0.07)	7.23 (0.15)	64.69 (1.91)	4.95 (0.25)	0.51 (0.03)
37.11	5.25	3.93 (0.12)	3.38 (0.11)	7.91 (0.09)	66.89 (2.23)	4.37 (0.14)	0.57 (0.02)
38.85	5.50	4.29 (0.28)	3.68 (0.25)	7.79 (0.38)	71.72 (5.96)	4.74 (0.57)	0.53 (0.06)

The U_s–u_p relationship for stack 2 is shown in Fig. 3 (red points). For stack 2, the shock velocity was determined in the following manner. The breakout times in the VISAR data were used to calculate the transit time through the SLG and Kapton. The time at which the shock breaks out into the SLG/Al/MgO interface was determined from the time of first fringe motion in both the VISAR1 and VISAR2. This was then corrected for the drive laser incident timing (t_0) using calibration files taken in the beginning of the day where a small amount of the drive laser light was allowed to directly pass through the VISAR legs and allowed to interfere. Therefore, the shock breakout time, i.e., the shock transit time through the Kapton, glue layers, and the SLG to the SLG/Al/MgO was determined. The shock velocities through Kapton for the incident laser energies were obtained from previous experiments performed at MEC[1,5] and were used to calculate the transit time through the Kapton layer. This Kapton transit time was subtracted from the shock breakout time to obtain the transit time through SLG. The shock velocity (U_s) for SLG was then calculated from the SLG transit time and the known sample thickness through which the shock transited. Note that the glue thicknesses were higher for stack 2 compared to stack 1. In order to account for the error due to glue thickness (0–10 μm), an average glue layer of 5 μm with a spread of 0–10 μm was assumed for the calculations. The epoxy glue and the polyimide ablator were assumed to have similar shock speeds in determining the shock transit time through it. The U_s–u_p relationship fit obtained from the stack 1 measurements were used as the Hugoniot for analysis of the stack 2 samples.

For stack 2 geometry, the SLG/Al/MgO interface particle velocity was measured after refractive index correction for the MgO window (n = 1.773 ± 0.016[10]) and corresponded to the reshocked state inside the SLG. To obtain the pressure–particle velocity (P–u_p) state in the SLG stack 2 samples, the SLG Hugoniot obtained from stack 1 measurements was impedance matched to the MgO Hugoniot obtained from the Los Alamos Shock Hugoniot databook by S.P. Marsh.[11] When the shock moves from SLG to MgO, a reshock wave is sent back into the SLG. The conservation equations dictate that the pressure and particle velocity are conserved across the contact interface between the MgO standard and the SLG sample. Therefore the pressure–particle velocity (P–u_p) state for the reshocked SLG and the shocked MgO must be the same.[9,12] Impedance matching was done by reflecting the SLG Hugoniot across the MgO Hugoniot (shocked state) at the measured interface particle velocity (reshocked state) in the pressure–particle velocity (P–u_p) space. The shocked state was then obtained from the point of intersection between the forward-facing SLG Hugoniot and the reflected SLG Hugoniot.[9,12] The density and the volume compression

TABLE II. Summary of the drive laser average intensity, drive laser energy, u_p, U_s, pressure, density, and volume compression results obtained for SLG sample stack 2 compressed by FT 10 ns pulse with 250 μm spot size.

|	Experimental quantities		Obtained from impedance matching		Calculated from transit time	Calculated in-material quantities	
Energy (J)	Intensity (TW/cm^2)	Interface u_p (km/s)	SLG pressure (GPa)	SLG u_p (km/s)	SLG U_s (km/s)	Density (g/cm^3)	Volume compression
19.20	3.91	3.21 (0.09)	89.22 (3.67)	4.12 (0.10)	8.64 (1.13)	4.81 (1.36)	0.52 (0.15)
33.13	6.75	3.83 (0.12)	117.00 (5.45)	4.81 (0.13)	9.66 (1.15)	5.01 (1.34)	0.50 (0.13)
42.22	8.61	4.94 (0.05)	175.20 (2.86)	6.03 (0.05)	10.79 (1.35)	5.71 (1.77)	0.44 (0.14)
59.56	12.1	6.54 (0.06)	277.10 (4.37)	7.76 (0.07)	14.58 (2.08)	5.39 (1.81)	0.47 (0.16)
58.10	11.8	7.06 (0.08)	315.90 (5.29)	8.33 (0.08)	14.58 (2.08)	5.88 (2.13)	0.43 (0.16)
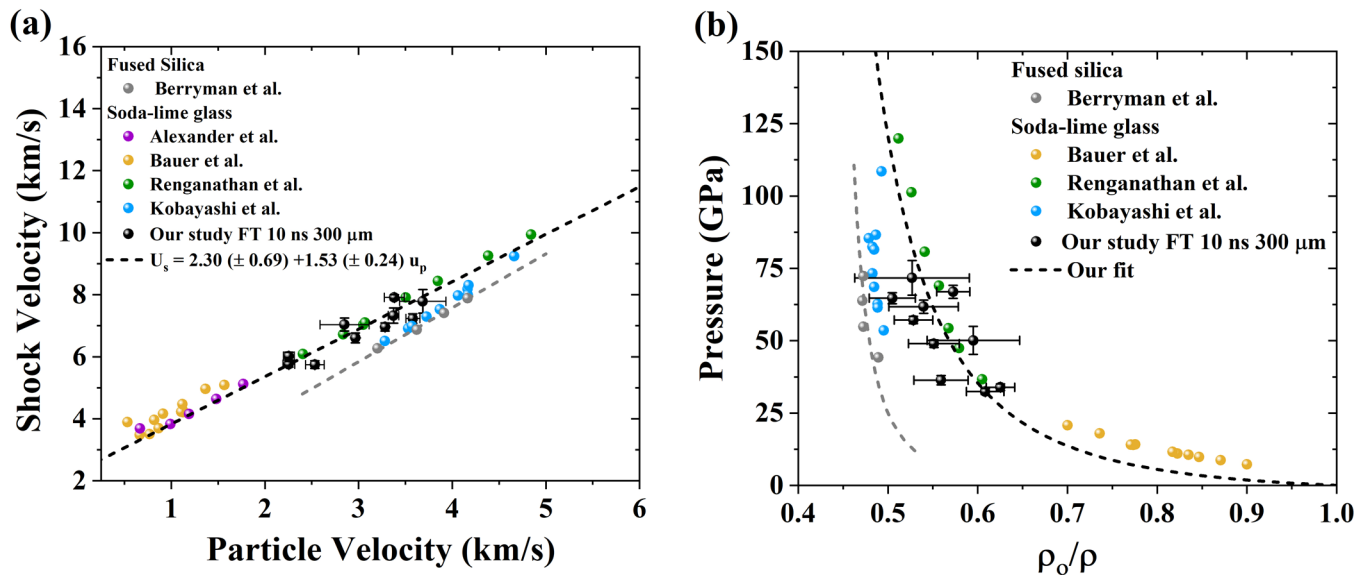
FIG. 4. (a) U_s–u_p relationship obtained from our study in comparison with the literature.[2,4,14–16] (b) Pressure vs volume compression calculated from U_s–u_p relationship compared with the literature.[2,14–16]

were obtained from Eqs. (2) and (3). The summary of all the shots including the drive laser average intensity, drive laser energy, U_s, u_p, and pressure (P) of samples in stack 2 geometry shock compressed by a $250 \mu m$ spot size FT 10 ns pulse is presented in Table II.

IV. DISCUSSION

Figure 4 compares the measured U_s–u_p and pressure vs volume relationship with the previous studies on SLG and fused silica (FS) primarily obtained from parallel plate impact measurements. Note that the U_s–u_p relationship obtained from Fig. 3 was used to calculate the fit shown in Fig. 4(b). We also calculated the strain rate using Eq. (5) similar to calculations performed by Smith et al.,[13]

$$\frac{d\mu}{dt} = \frac{1}{\rho}\frac{d\rho}{dt},$$ (5)

where μ is the strain, ρ is the density of the shocked sample, and dt is the shock rise time. Using this, we obtained a strain rate of 1.33–1.90 ns^{-1} for the pressure range of 50–315 GPa. In spite of differences in the strain rate for gas gun compared to laser-driven shock impact, the obtained fit for U_s-u_p matches well with the literature values.[2,4,14–16] The pressure vs volume compression ($\frac{\rho_o}{\rho}$) were also seen to match with studies by Renganathan et al.[2] and Alexander et al.[4]

Figures 3 and 4 show that U_s–u_p is linear upto 315 GPa within the experimental error bars. Furthermore, the shocked SLG is seen to compress smoothly from 30 to 70 GPa without any sudden changes in the compressibility. Specifically, in comparison to FS, SLG is seen to be more compressible with increasing stress indicated by pressure vs volume dependence [Fig. 4(b)]. No noticeable discontinuity observed in the U_s–u_p or the calculated pressure

vs volume compressibility indicates toward lack of phase transition or polymorphic behavior in the SLG sample. This behavior is also consistent with the recent parallel plate impact studies done by Renganathan et al.[2] However, additional measurements, such as longitudinal modulus and sound velocity calculations, along with x-ray diffraction/pair distribution function analysis can further confirm the structural changes (i.e., continuous transition to a high density phase) under laser-driven shock compression.

The lack of sudden changes in the pressure vs volume compression ($\frac{\rho_o}{\rho}$), as well as the higher compressibility of shocked SLG in comparison with FS, indicates that the presence of Na$^+$, Ca^{2+}, and Mg^{2+} cations in SLG might impede the phase transformation to stishovite that is observed in fused silica. It is also possible that SLG undergoes a smaller change in volume during the transformation as observed by Renganathan et al.[17] for a pressure range of 52–58 GPa, which shows solid to liquid transformation marked by an abrupt decrease in sound velocities and moduli. Our studies, thus, show that composition (i.e., the addition of Na$^+$ Ca^{2+}) can strongly influence the shock compression behavior of silicate glasses. While we focused on SLG in this study, studying the behavior of other silicate glasses, such as borosilicate, aluminum borosilicate, etc., which contain network former cations (B^{3+}, Al^{3+}), in the same pressure range would provide further information on how the additional oxides (both network formers and modifiers) influence phase transformations in the silicate glasses.

V. CONCLUSION

The dynamic response of soda-lime silicate glass was studied using laser-driven shock compression up to 315 GPa to investigate the effect of network modifying cations. The measured U_s–u_p

relationship was seen to agree well with the literature, indicating that shock behavior is similar in SLG for both laser-driven shock and gas gun studies. The lack of kinks or discontinuities in U_s–u_p data within the error bars suggests there is no phase transition to stishovite up to 70 GPa, contrary to that observed for fused silica. These observations show that the presence of network modifiers impedes the phase transition to crystalline stishovite. This agrees well with the recent observations made in parallel plate impact measurements in the soda-lime glass indicating that despite different strain rates for gas gun and laser shock, the material behavior is similar. Detailed dynamic diffraction measurements are required to unequivocally identify the phases present during laser-driven shock compression.

SUPPLEMENTARY MATERIAL

The VISAR data for all the stack 1 and stack 2 SLG samples are shown in the supplementary material.

ACKNOWLEDGMENTS

AUTHOR DECLARATIONS

Conflict of Interest

The authors have no conflicts to disclose.

Author Contributions

Meera Madhavi: Data curation (equal); Formal analysis (equal); Investigation (equal); Methodology (equal); Writing – original draft (equal); Writing – review & editing (equal). **Rahul Jangid:** Investigation (supporting). **Joyce Christiansen-Salameh:** Investigation (supporting). **Yu Hsing Cheng:** Investigation (supporting). **Pooja Rao:** Investigation (supporting). **Jianheng Li:** Investigation (supporting). **Surya Teja Botu:** Investigation (supporting). **Spencer Jeppson:** Investigation (supporting). **Jugal Mehta:** Investigation (supporting). **Scott Smith:** Investigation (supporting). **Jared T. Isobe:** Investigation (supporting). **Sovanndara Hok:** Investigation (supporting). **Rahul Saha:** Investigation (supporting). **Eric Cunningham:** Investigation (supporting); Methodology (equal); Resources (equal). **Philip Heimann:** Investigation (supporting); Methodology (equal); Resources (equal). **Dimitri Khaghani:** Investigation (supporting); Methodology (equal); Resources (equal). **Hae Ja Lee:** Investigation (supporting); Methodology (equal); Resources (equal). **D. K. Spaulding:** Investigation (supporting); Methodology (equal); Supervision (supporting); Visualization (supporting). **Danae N. Polsin:** Investigation (supporting); Methodology (equal); Software (equal); Visualization (supporting). **Arianna E. Gleason:** Investigation (equal); Methodology (equal); Supervision (supporting); Visualization (supporting). **Roopali Kukreja:** Funding acquisition (equal); Investigation (equal); Methodology (equal); Supervision (equal); Visualization (equal); Writing – original draft (equal); Writing – review & editing (equal).

DATA AVAILABILITY

The data that support the findings of this study are available from the corresponding author upon reasonable request.

REFERENCES

[1] A. E. Gleason, C. A. Bolme, H. J. Lee, B. Nagler, E. Galtier, R. G. Kraus, R. Sandberg, W. Yang, F. Langenhorst, and W. L. Mao, "Time-resolved diffraction of shock-released SiO$_2$ and diaplectic glass formation," Nat. Commun. **8**(1), 1481 (2017), ISSN: 2041-1723.

[2] P. Renganathan, T. S. Duffy, and Y. M. Gupta, "Hugoniot states and optical response of soda lime glass shock compressed to 120 GPa," J. Appl. Phys. **127**(20), 205901 (2020), ISSN: 0021-8979, 1089-7550.

[3] C. S. Alexander, L. C. Chhabildas, W. D. Reinhart, and D. W. Templeton, "Changes to the shock response of fused quartz due to glass modification," Int. J. Impact Eng. **35**(12), 1376–1385 (2008), ISSN: 0734743X.

[4] C. S. Alexander, L. C. Chhabildas, D. W. Templeton, M. Elert, M. D. Furnish, R. Chau, N. Holmes, and J. Nguyen, "The Hugoniot elastic limit of soda-lime glass," AIP Conference Proceedings **955**, 733-738 (2007).

[5] A. E. Gleason, C. A. Bolme, H. J. Lee, B. Nagler, E. Galtier, D. Milathianaki, J. Hawreliak, R. G. Kraus, J. H. Eggert, D. E. Fratanduono, G. W. Collins, R. Sandberg, W. Yang, and W. L. Mao, "Ultrafast visualization of crystallization and grain growth in shock-compressed SiO$_2$," Nat. Commun. **6**(1), 8191 (2015), ISSN: 2041-1723.

[6] L. M. Barker and R. E. Hollenbach, "Laser interferometer for measuring high velocities of any reflecting surface," J. Appl. Phys. **43**(11), 4669–4675 (1972), ISSN: 0021-8979, 1089-7550.

[7] L. M. Barker and K. W. Schuler, "Correction to the velocity-per-fringe relationship for the VISAR interferometer," J. Appl. Phys. **45**(8), 3692–3693 (1974), ISSN: 0021-8979, 1089-7550.

[8] L. M. Barker, "Laser interferometry in shock-wave research: Author reviews the various types of interferometer that have been applied to shock-wave research and describes the present capabilities and limitations," Exp. Mech. **12**(5), 209–215 (1972), ISSN: 0014-4851, 1741-2765.

[9] J. W. Forbes, *Shock Wave Compression of Condensed Matter: A Primer* (Springer, Berlin, 2012), ISBN: 978-3-642-32534-2 978-3-642-32535-9.

[10] D. E. Fratanduono, J. H. Eggert, M. C. Akin, R. Chau, and N. C. Holmes, "A novel approach to Hugoniot measurements utilizing transparent crystals," J. Appl. Phys. **114**(4), 043518 (2013), ISSN: 0021-8979, 1089-7550.

[11] "LASL shock Hugoniot data," in *LosAlamos Series on Dynamic Material Properties*, edited by Stanley P. Marsh (University of California Press, Berkeley, 1980), ISBN: 978-0-520-04008-3.

[12] M. A. Barrios, D. G. Hicks, T. R. Boehly, D. E. Fratanduono, J. H. Eggert, P. M. Celliers, G. W. Collins, and D. D. Meyerhofer, "High-precision measurements of the equation of state of hydrocarbons at 1–10 Mbar using laser-driven shock waves," Phys. Plasmas **17**(5), 056307 (2010), ISSN: 1070-664X, 1089-7674.

[13] R. F. Smith, J. H. Eggert, D. C. Swift, J. Wang, T. S. Duffy, D. G. Braun, R. E. Rudd, D. B. Reisman, J.-P. Davis, M. D. Knudson, and G. W. Collins, "Time-dependence of the alpha to epsilon phase transformation in iron," J. Appl. Phys. **114**(22), 223507 (2013), ISSN: 0021-8979, 1089-7550.

[14]T. Kobayashi, T. Sekine, O. V. Fat'yanov, E. Takazawa, and Q. Y. Zhu, "Radiation temperatures of soda-lime glass in its shock-compressed liquid state," J. Appl. Phys. **83**(3), 1711–1716 (1998), ISSN: 0021-8979, 1089-7550.

[15]S. Bauer, F. Bagusat, E. Strassburger, M. Sauer, and S. Hiermaier, "New insights into the failure front phenomenon and the equation of state of soda-lime glass under planar plate impact," J. Dyn. Behav. Mater. **7**(1), 81–106 (2021), ISSN: 2199-7446, 2199-7454.

[16]E. J. Berryman, J. M. Winey, Y. M. Gupta, and T. S. Duffy, "Sound velocities in shock-synthesized stishovite to 72 GPa," Geophys. Res. Lett. **46**(23), 13695–13703, https://doi.org/10.1029/2019GL085301 (2019), ISSN: 0094-8276, 1944-8007.

[17]P. Renganathan, T. S. Duffy, and Y. M. Gupta, "Sound velocities in shock-compressed soda lime glass: Melting and liquid-state response," Phys. Rev. B **104**(1), 014113 (2021), ISSN: 2469-9950, 2469-9969.